doi:10.3788/gzxb20184709.0913003

基于硅基光学相控阵的大范围二维光束扫描

李中宇[1,2,3],章羚璇[1,2,3],曾超[1,2,3],杜书剑[1,2,3],葛志强[1,2,3],谢鹏[1,2,3],张其浩[1,2,3],王国玺[1,2,3],孙笑晨[1,2],米磊[1],张文富[1,2,3]

(1 中国科学院西安光学精密机械研究所 瞬态光学与光子技术国家重点实验室,西安 710119)

(2 中国科学院大学,北京 100049)

(3 中国科学院西安光学精密机械研究所 中英联合微纳光子学研究中心,西安 710119)

摘 要:基于硅基光学相控阵,提出一种结合了相位控制和不同周期光栅发射器的点阵扫描法,以实现大范围的二维光束扫描.对光束扫描装置进行仿真计算,结果表明,仅使用单波长的光源即可实现 120°×100°的扫描范围和超过 16×400 个可分辨点.此光束扫描装置在应用时,同一时刻仅需要一部分有源器件工作,降低了相调所需的电能耗.所提方法为实现大范围、低成本和低功耗的二维光束扫描装置提供了一种可能的解决方案,尤其适用于低成本的固态激光雷达.

关键词:光电子学;光学相控阵;光栅;绝缘体上硅;光束扫描;激光雷达

中图分类号:TN256 **文献标识码**:A **文章编号**:1004-4213(2018)09-0913003-9

Ultra-wide Two-dimensional Beam Steering by Silicon Integrated Optical Phased Array

LI Zhong-yu[1,2,3], ZHANG Ling-xuan[1,2,3], ZENG Chao[1,2,3], DU Shu-jian[1,2,3], GE Zhi-qiang[1,2,3], XIE Peng[1,2,3], ZHANG Qi-hao[1,2,3], WANG Guo-xi[1,2,3], SUN Xiao-chen[1,2], MI Lei[1,2], ZHANG Wen-fu[1,2,3]

(1 *State Key Laboratory of Transient Optics and Photonics, Xi'an Institute of Optics and Precision Mechanics, Chinese Academy of Sciences, Xi'an* 710119, *China*)

(2 *University of Chinese Academy of Sciences, Beijing* 100049, *China*)

(3 *China-UK Joint Research Center of Micro/Nano Photonics, Xi'an Institute of Optics and Precision Mechanics, Chinese Academy of Sciences, Xi'an* 710119, *China*)

Abstract: An alternative approach to realize 2D beam steering with ultra-wide range by silicon integrated optical phased array is proposed. A dot matrix scanning method, using the phase control and grating emitters with different periods, is conceived to design the optical phased array device without the requirement of tunable lasers. Simulations demonstrate an ultra-wide steering range up to 120°×100°, together with over 16×400 resolvable points by using a single-wavelength laser. Moreover, the designed optical phased array device demands only a part of active elements working simultaneously, which benefits to reduce the electrical power consumption. The proposed approach provides a promising solution for wide-angle, low-cost, and low-power consumption 2D beam steering devices, especially suitable for solid-state light detection and ranging systems.

Key words: Optoelectronics; Optical phased array; Grating; Silicon-on-insulator; Beam steering; LiDAR

OCIS Codes: 130.3120; 130.0250; 230.7370; 250.3140

Foundation item: The National Natural Science Foundation of China (Nos. 61475188, 61705257, 61405243), the Strategic Priority Research Program of the Chinese Academy of Sciences (No. XDB24030600)

First author: LI Zhong-yu(1992—),male, M.S. degree candidate, mainly focuses on integrated photonics devices. Email: lizhongyu2015@opt.cn

Supervisor (Contact author): ZHANG Wen-fu(1982—), male, professor, Ph.D. degree, mainly focuses on integrated photonics & nanophotonics. Email: wfuzhang@opt.ac.cn

Received: Apr.3, 2018; **Accepted**: Jun.8, 2018

0 Introduction

Traditional mechanical optical beam scanners, e. g. rotating mirror, are expensive and sensitive to mechanical shocks and ambient temperature[1]. Further investigations include the use of micro-electro-mechanical-system[2] and liquid-crystal-based spatial light modulators[3]. However, these beam steering systems exhibit a comparatively slow scanning speed[3]. With the development of the CMOS-compatible silicon photonic technology, silicon integrated Optical Phased Array (OPA) on chip has been demonstrated to overcome the disadvantages of aforementioned beam steering methods[4]. The technology of chip-based OPA shows a wide range of applications in Light Detection and Ranging (LiDAR), optical communications, and holography[5].

Two-dimensional (2D) beam steering by silicon integrated OPA can be realized with two methods. One employs phase control in one direction and tunable laser in the other direction[6-11]. By using this method, POULTON C V, et al. presented the first demonstration of solid-state LiDAR with chip-based OPA for 2D beam steering[11]. A total steering range of $46°\times36°$ was achieved with operation wavelength tuning from 1 454 nm to 1 641 nm. However, tunable laser is expensive, and in particular its tuning range limits the steering range of OPA. The other method is using phase control in both directions[12-20]. For instance, an 8×8 active OPA consisting of 64 emitters was developed by SUN J, et al, which can achieve dynamic 2D beam steering[12]. In general, this type of 2D OPA requires$N\times N$ independent active phase tuning and beam emitting elements. As the beam width scales inversely with $N\times N$, in order to get a narrow beam divergence, the amounts of phase tuners and light emitters are always very large, which brings a big challenge to manufacture, power consumption, and control electronics[19]. Therefore, high-performance chip-based OPA with large steering range, single-wavelength source, and low power consumption is desired for 2D beam steering applications[5].

In this paper, we propose an alternative approach to realize 2D wide-angle beam steering. In our proposal, grating emitters with different periods are exploited to realize beam steering in one direction, which is called period control in the following discussion. By combining period control with phase control, an ultra-wide steering range of $120°\times100°$ is achieved with over 16×400 resolvable points. Such a wide steering range is obtained with only a single-wavelength laser, which can reduce the cost of the chip-based OPA devices. Furthermore, due to merely requiring a part of switching elements and phase tuners working simultaneously, our approach can decrease the power consumption and control electronics complexity of the silicon integrated OPA devices.

1 Structure and model

1.1 Design of the silicon integrated OPA device

As shown in Fig. 1, an $N\times M$ silicon integrated OPA device is proposed and designed, where N is the amount of grating emitters and M is the amount of antennas in one emitter (for clarity, only 4×4 structure is illustrated in this Fig). The proposed OPA device is composed of five parts: grating coupler, switch array, splitter array, resistive heaters array, and grating emitter array. Each grating emitter has M grating antennas with the same grating period. The grating coupler is used to couple the light from an off-chip single-wavelength laser into on-chip waveguide. The fiber-chip grating couplers have been utilized to couple 1 310 nm light into waveguides with a coupling efficiency of -1.9 dB[21]. The switch array ($1\times N$), consisting of Mach-Zehnder electro-optic switching elements, functions to select the light into one of the N channels and a thermo-optic switch with on-off ratio of ~23 dB have been reported in the previous investigation, at switching power of 4.35 mW[22].

The splitterarray based on Multi-Mode Interferometer (MMI) splits the light of one channel into M channels. The resistive heaters array permits independently phase controlling of each channel. The heater is a strip of metal running alongside each ridge waveguide and contacted by electrodes, which has been demonstrated with a phase-shifting efficiency of 215 ± 15 mW/π[6]. The grating emitters deliver the light beams into different directions in the far field. Each emitter has M grating antennas, which is in agreement with the amount of heater array. As represented in Fig. 1, the emitted light beam traces out the fan-shaped

directions and is steerable using period control (θ axis) and phase control (ψ axis).

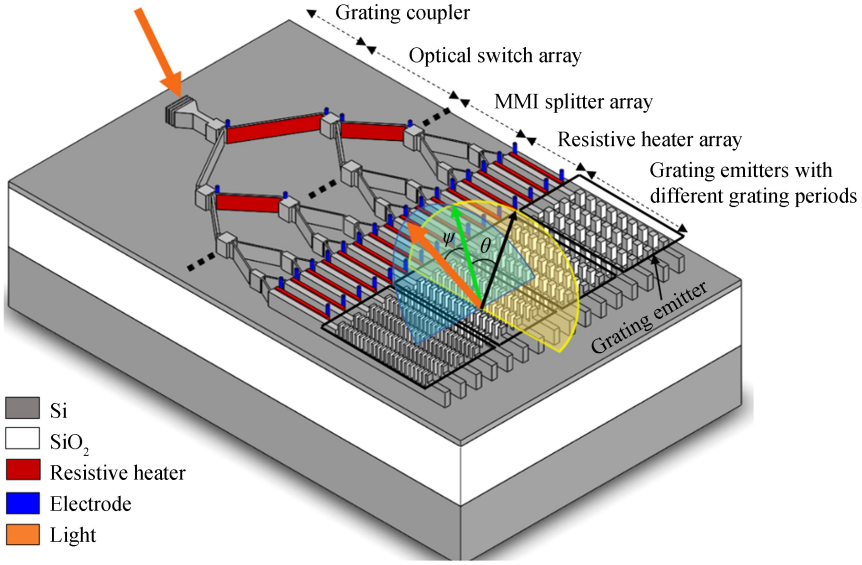

Fig.1 Structural model of silicon integrated OPA device

1.2 Characterization of single grating antenna

The grating antennas are etched at the end of the ridge waveguide, with 50% duty cycle. The ridge waveguide with a slab height of 100 nm is patterned in the SOI substrate. The SOI has 250 nm top silicon (Si) and 1 μm silica (SiO_2) layer. To achieve large steering range in the ψ axis, the wide-angle radiation from a single grating antenna is in demand. The radiation range ($2\psi_r$) of a single antenna in the ψ axis can be roughly estimated by[23]

$$2\psi_r = \frac{2\lambda_0}{\pi \cdot w} \tag{1}$$

where w is the width of grating antenna and λ_0 is the operation wavelength. The 3D Finite-Difference Time-Domain (FDTD) method is carried out to simulate the performance of single grating antenna with λ_0 =1 310 nm, w=1 μm, d=1 μm, Λ=450 nm (grating period) and a slab height of 100 nm. As illustrated in Fig. 2, the 3 dB radiation range is over 90° in the ψ axis, indicating that this grating antenna can be used to achieve a large steering range in the ψ axis.

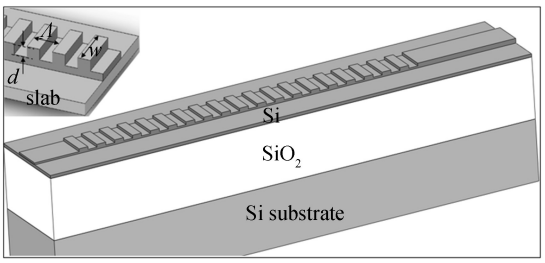

(a) Grating antenna structure, the inset presents the structure drawing of single grating antenna at a different angle

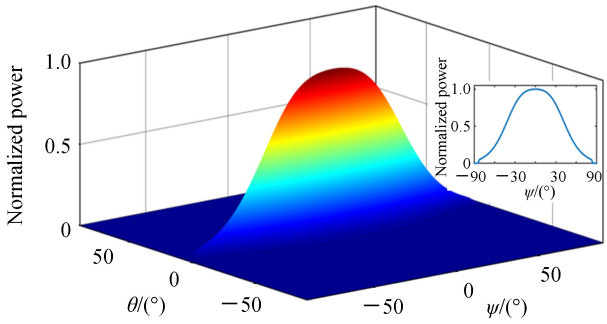

(b) Far-field pattern of the single grating antenna, the inset shows the cross-section of the far-field pattern at θ=0°

Fig.2 Schematics of designed grating antenna structure and simulation result

For ageneral grating antenna, the beam width in the θ axis is determined by the propagation distance, which is the effective length of grating antenna where the light emits out completely[24]. The FDTD simulations of single grating antenna with Λ=490 nm and different etch depth d is shown in Fig. 3. Fig indicates that shallow etched grating antenna leads to a smaller beam width because of a longer propagation distance, whereas deep etched grating antenna enables strong perturbation, resulting in a shorter propagation distance as well as a wider beam width. In general, the silicon integrated OPA devices require smaller beam width to achieve more resolvable points[8]. However, grating antenna with an extremely

shallow etch depth causes to a lower coupling efficiency. Fig. 3(c) is the cross-section of the far-field pattern at $\psi=0°$ with d from 50 nm to 130 nm, by the increment of 10 nm. Fig. 3(d), coupling efficiency and FWHM of the beams emitted from antennas with d from 30 nm to 130 nm, by the increment of 5 nm. The Full-Width at Half-Maximum (FWHM) stands for the width of emitted beam. According to the simulation results in Figs. 3(c) and 3(d), in the following discussion, a grating antenna with the etch depth $d=70$ nm is chosen to balance the conflict between coupling efficiency and beam width.

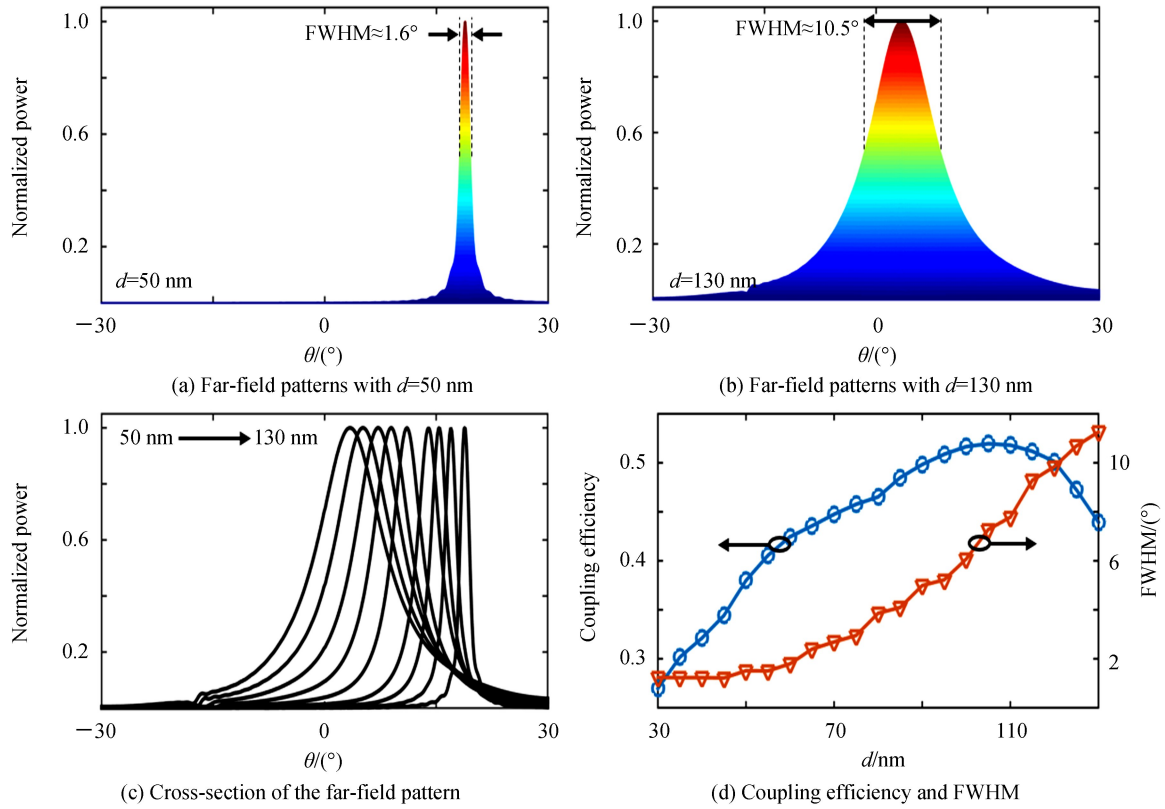

Fig.3 Simulation results of single grating antenna with different d

2 Results and discussion

Tocharacterize the beam steering performances of the proposed OPA device, a dot matrix scanning method is conceived to investigate the dynamics of the phase and period controls. In this section, we firstly discuss the period- and phase-controlled beam steering in two different axes (θ and ψ as shown in Fig. 1) respectively, and then an ultra-wide 2D beam steering is obtained by simultaneously controlling of phase and period.

2.1 Period-controlled beam steering in the θ axis

The emission angle of a grating antenna in the θ axis is governed by[25]

$$\sin\theta=\frac{n_{\mathrm{eff}}\cdot\Lambda-\lambda_0}{\Lambda} \tag{2}$$

where n_{eff} is the effective index of the grating. Eq. (2) indicates that θ highly depends on the grating period Λ. Therefore, grating period provides an additional route to achieve beam steering in the θ axis instead of using wavelength-tunable lasers, which have been widely applied in traditional OPA devices[6-11].

Fig. 4(a) illustrates the normalized emission profiles of grating antennas with 32 different periods from 340 nm to 650 nm by the increment of 10 nm. It can be seen that the emission angle θ covers range from −64.8° to 58.2° under condition that the scanning point is resolvable, which is much larger than previously reported OPA devices[12,17]. Fig. 4(b) presents the coupling efficiency of grating antennas with different periods. The scope of the coupling efficiency is from 0.23 to 0.44, while the efficiency is large than 0.4 with periods from 410 nm to 540 nm. In addition, as shown in Fig. 4(c), the beam width in the θ axis ranges from 1.4° to 11.1° with a mean width of 3°, the $2\psi_r$ of a single antenna in the ψ axis are from 37.0°

to 92.7° with a mean radiation range of 73.5°.

Under the control of optical switch array, only one of the grating emitters (each has 16 antennas) works at a time, and the light beam emits into the certain direction (corresponding to the grating period of the working emitter). Consequently, by the proposed period-controlled route, the ultra-wide steering range up to 120° can be achieved in the θ axis with great ease. Furthermore, the resolvable points in the θ axis are 16 in proposed integrated OPA device, which are determined by the amount of grating emitters with different periods. It is also possible to substantially improve the resolvable points by adopting more grating emitters with different periods, shallower-etched grating antennas or tunable lasers.

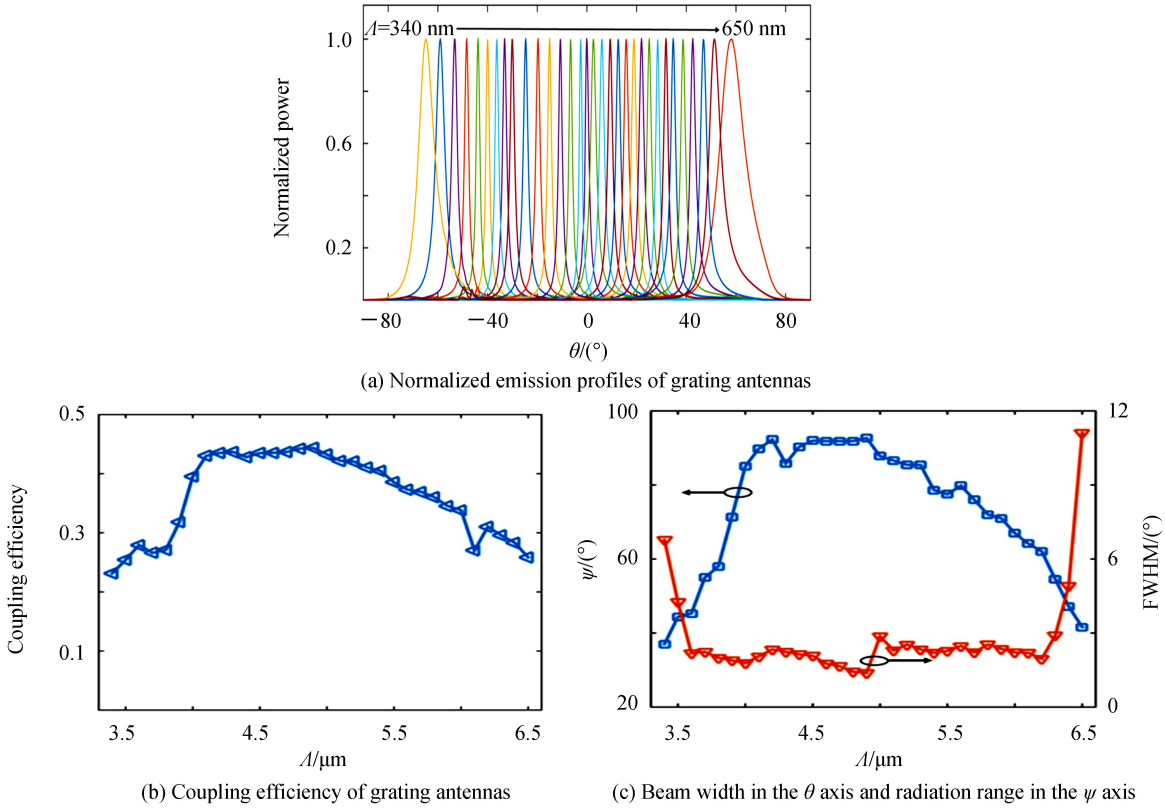

(a) Normalized emission profiles of grating antennas

(b) Coupling efficiency of grating antennas

(c) Beam width in the θ axis and radiation range in the ψ axis

Fig.4 Characterization of period-controlled beam steering in the θ axis

2.2 Phase-controlled beam steering in the ψ axis

Different from the θ axis, beam steering in the ψ axis is accomplished by the phase control, as presented schematically in Fig. 1. For the grating emitter with uniformly spaced antennas, its emission angle in the ψ axis is expressed as[6]

$$\sin\psi=\frac{\lambda_0\cdot\Delta\varphi}{2\pi\cdot S} \tag{3}$$

where $\Delta\varphi$ and S are the phase increment and space separation between adjacent grating antennas, respectively. The beam width can be estimated as[26]

$$\psi_{\mathrm{div}}\approx\frac{0.88\lambda_0}{M\cdot S\cdot\cos\psi} \tag{4}$$

From Eqs. (3) and (4), it is found that the steering range $2\psi_{\mathrm{steer}}$ (when $\Delta\varphi=\pm\pi$) and beam width ψ_{div} are both related to the space separation S. In practical applications, OPA devices usually require large steering range and small beam width. Fig 5 presents the FDTD simulation results of the grating emitters as functions of space separation and phase increment. When $\Delta\varphi=\pi$, the steering range $2\psi_{\mathrm{steer}}$ decreases with increase of S, as represented in Fig. 5(a); When $\Delta\varphi=0$, the results in Figs. 5(b) and 5(c) prove that the beam width ψ_{div} also decreases with increase of S. The simulations agree well with the theoretical analyses that there exists a trade-off between steering range and beam width in terms of space separation. To achieve wider steering range, a narrower space separation is required at the cost of resolvable points, which

is inversely proportional to beam width. Noteworthy, when the space separation is larger than $\lambda_0/2$, as shown in Fig. 5(b), the grating lobes emerge, which originate from constructive interference between light beams from different antennas[10]. Such grating lobes decrease the steering range and Side-Mode Suppression Ratio (SMSR), which limit applications of OPA devices[6,10].

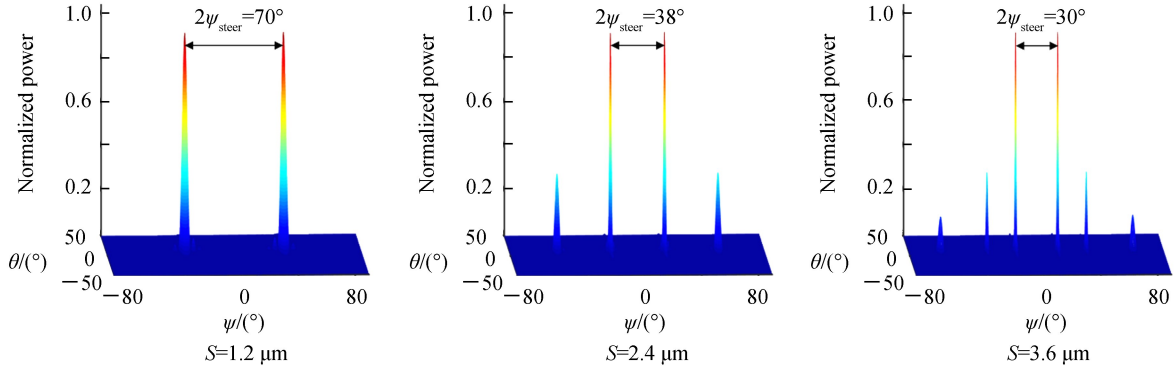

(a) Far-field pattern of grating emitters with $\Delta\varphi=\pi$

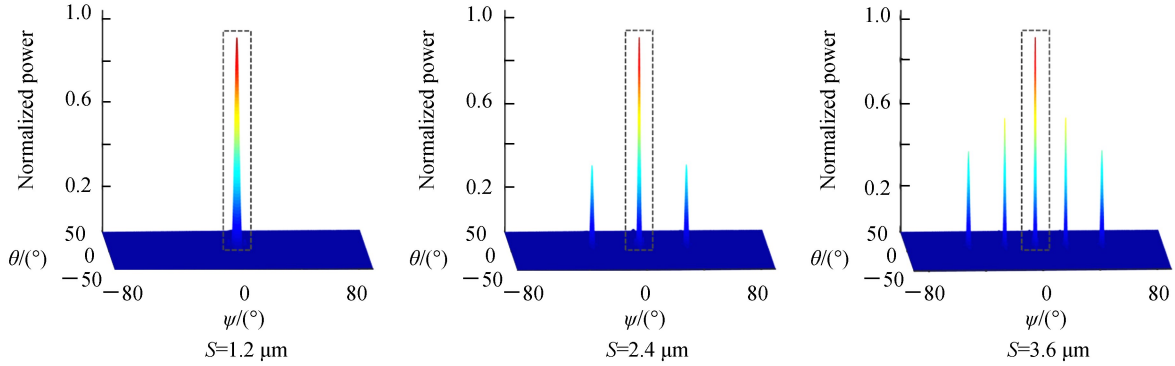

(b) Far-field pattern of grating emitters with $\Delta\varphi=0$

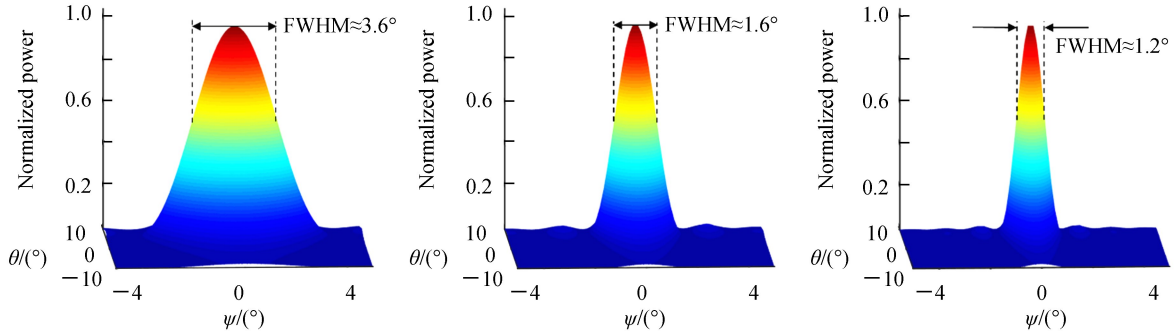

(c) Close-up view of the main lobe (dash box) in (b)

Fig.5 Characterization of phase-controlled beam steering in the ψ axis with $S=1.2$, 2.4, and 3.6 μm

The physical model of OPA is the multi-slit Fraunhofer diffraction. Assuming $\alpha=w\cdot\sin(\psi/2)\cdot\frac{2\pi}{\lambda}$, for a uniform grating emitter without additional $\Delta\varphi$, the far-field intensity can be expressed as

$$I(\psi)=\left(\frac{\sin\alpha}{\alpha}\right)^2\left[\frac{\sin\left(\frac{M\pi}{\lambda}S\sin\psi\right)}{\sin\left(\frac{\pi}{\lambda}S\sin\psi\right)}\right]^2 \tag{5}$$

The position of grating lobes is governed by

$$M\cdot S\cdot\sin\psi\cdot\frac{\pi}{\lambda}=\pm 2m\pi\quad(m=1,2,3\cdots\cdots) \tag{6}$$

For the non-uniformly spaced grating emitter, the space separation S is inhomogeneous, so the constructive interference condition is not satisfied, which means that the grating lobes are suppressed and hence the SMSR can be improved. For comparisons, the grating emitters with uniform and non-uniform

space separations are investigated respectively. The grating emitters are composed of the aforementioned grating antennas, with $w=1$ μm, $\Lambda=490$ nm, and $d=70$ μm. The emission profiles of uniform OPA with $\psi=0°$ and $S=4.78$ μm is represented in Fig. 6(a), showing that the steering range of uniform OPA is limited by grating lobes. The largest steering range of the main lobe is half of the distance between two first grating lobes. When the main lobe locates at $\psi=0$, the first grating lobe at $\psi\sim7.8°$. If main lobe steers to $\psi=10°$, the first grating lobe takes place of the original main lobe. By using non-uniform OPA, the constructive interference no longer happens, resulting in suppressing of grating lobes, as illustrated in Fig. 6(b). The non-uniform space separations S are generated by a hill-climbing algorithm ($S=6.4$, 6.3, 1.5, 3, 2.1, 3.8, 2, 4.7, 3.9, 5.5, 2.8, 3.4, 7.1, 8.5, and 7.4 μm). Continuously, large range beam steering is simulated and the corresponding results, plotted in Fig. 6(c), demonstrate a wide steering range of 100° with the SMSR over 3.83 dB. The FWHM of the main lobe is estimated to be 0.206° ($\psi=0°$) and 0.267° ($\psi=50°$), and the mean FWHM is 0.229°, which indicates that more than 400 resolvable points are obtained in the ψ axis. It is possible to further improve the SMSR by increasing the number of antennas in a grating emitter, under the permission of process.

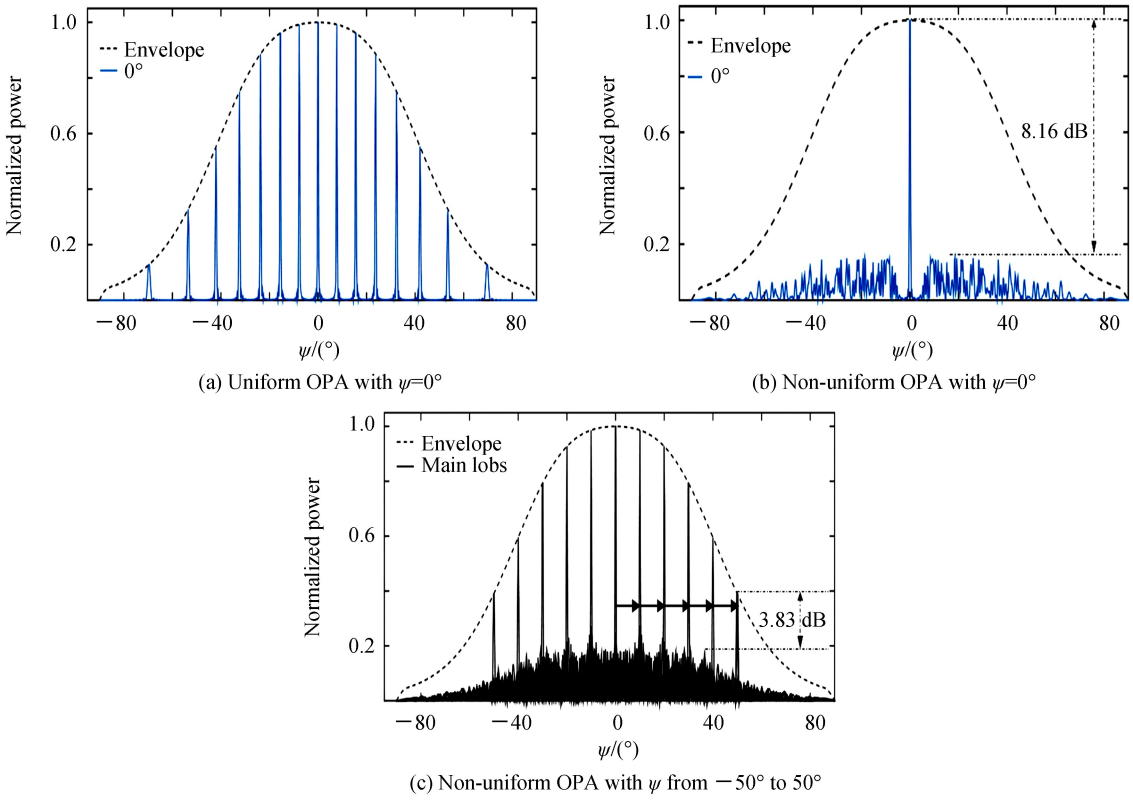

(a) Uniform OPA with ψ=0°

(b) Non-uniform OPA with ψ=0°

(c) Non-uniform OPA with ψ from −50° to 50°

Fig.6 Suppression of grating lobes using non-uniform OPA

2.3 Ultra-wide 2D beam steering

Based on the aforementioned analyses, a 2D beam steering with ultra-wide range is achieved by the proposed silicon integrated OPA. The grating emitter arrays of the OPA model is composed of 16 emitters, and each emitter contains 16 grating antennas. The FDTD simulation results in Fig. 7 are carried out at periods $\Lambda=340$, 490, 650 nm with $\Delta\varphi$ varying as a function of the non-uniform separations. The five featured emission profiles correspond to different parameters: period Λ and phase $\Delta\varphi$ with the non-uniform separations S (the

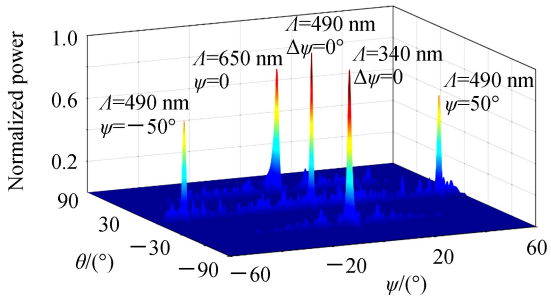

Fig.7 Two-dimensional beam steering performance of the proposed silicon integrated OPA devic

same as that in Fig. 6). The relationship between $\Delta\varphi$, ψ and S is governed by Eq. (3). Fig 7 demonstrates that the maximum steering ranges in the θ and ψ axes are up to 120° and 100° respectively, with over 16×400 resolvable points, when SMSR is larger than 3 dB. According to Eq. (1), the flatness of emission profiles in ψ axis is determined by width of grating antenna, whereas, as shown in Fig. 4(b), the flatness in θ axis is determined by the coupling efficiency of grating antennas with different periods. Therefore, a better flatness could be achieved by using a narrower grating antenna and the grating with periods corresponding to the similar coupling efficiency. Moreover, the amplitude modulation of incident light could also improve the flatness of emission profiles[19].

Compared with previously reported OPA devices, our device exhibits several advantages, such as possessing an ultra-wide steering range of 120°×100°, consuming lower electrical power, and only requiring a single-wavelength laser source, as shown in Table 1.

Table 1 Performance comparisons among our 2D OPA device and previously reported devices

Ref.	Laser source	Steering range ($\theta\times\psi$)	Beam width ($\theta\times\psi$)	Resolvable points ($\theta\times\psi$)	Amount of active elements working simultaneously	Experimental or theoretical
[6]	Tunable	20°×14°	0.6°×1.6°	33×9	16	Experimental
[7]	Tunable	20°×15°	1.2°×0.5°	16×30	16	Experimental
[9]	Tunable	3.6°×23°	0.6°×1°	6×23	31	Experimental
[10]	Tunable	17°×80°	0.14°×0.142°	120×500	128	Experimental
[11]	Tunable	46°×36°	0.85°×0.16°	54×225	50	Experimental
[15]	Single	30°×30°	10°×25°	3×1	4	Theoretical
[16]	Single	12°×12°	1.6°×1.6°	7×7	64	Experimental
Our work	Single	120°×100°	3°×0.229°	16×400	31	Theoretical

3 Conclusion

In summary, an alternative approach to realize 2D beam steering using silicon integrated OPA is proposed and demonstrated using a single-wavelength laser source. The dot matrix scanning method, combining period control with phase control, is conceived to improve steering range, reduce the power consumption, and avoid the requirement of tunable source. The simulation results prove that the proposed 16×16 OPA device can achieve an ultra-wide steering range up to 120°×100° and over 16×400 resolvable points. By only using a single-wavelength laser source, the proposed OPA device has been demonstrated to steer light beams in 2D directions, which overcome the limitation of tunable sources. Moreover, only 16 phase tuners and less than 15 switching elements are required to work simultaneously, which reduces the electrical power consumption. Therefore, our approach provides a promising solution for compact, wide-angle, low-power consumption 2D beam steering devices, especially suitable for solid-state LiDAR systems.

References

[1] SONG Yue-hui, SHI Gao-dong, LI Shi-chun, *et al*. Design of wavelength tunable lidar system[J]. *Acta Photonica Sinica*, 2017, **46**(10):1001001.

[2] CHAN T K, MEGENS M, YOO B W, *et al*. Optical beamsteering using an 8 × 8 MEMS phased array with closed-loop interferometric phase control.[J]. *Optics Express*, 2013, **21**(3):2807-2815.

[3] DAI Jing, ZHANG Min-ming, HE Yan, *et al*, Study on characteristics of a novel optical phased array based on liquid crystal[J]. *Acta Photonica Sinica*, 2014, **43**(2):223002.

[4] VAN A K, BOGAERTS W, JÁGERSKÁ J, *et al*. Off-chip beam steering with a one-dimensional optical phased array on silicon-on-insulator[J]. *Optics Letters*, 2009, **34**(9):1477-1479.

[5] HECK M J R. Highly integrated optical phased arrays: photonic integrated circuits for optical beam shaping and beam steering[J]. *Nanophotonics*, 2016, **6**(1):93-107.

[6] DOYLEND J K, HECK M J, BOVINGTON J T, *et al*. Two-dimensional free-space beam steering with an optical phased array on silicon-on-insulator[J]. *Optics Express*, 2011, **19**(22):21595.

[7] KWONG D, HOSSEINI A, COVEY J, *et al*. On-chip silicon optical phased array for two-dimensional beam steering. [J]. *Optics Letters*, 2014, **39**(4):941.

[8] YAACOBI A, SUN J, MORESCO M, *et al*. Integrated phased array for wide-angle beam steering.[J]. *Optics Letters*,

2014, **39**(15):4575-4578.

[9] HULME J C, DOYLEND J K, HECK M J R, *et al*. Fully integrated hybrid silicon two dimensional beam scanner[J]. *Optics Express*, 2015, **23**(5):5861-5874.

[10] FESHALI A, PHARE C T, HUTCHISON D N, *et al*. High-resolution aliasing-free optical beam steering[J]. *Optica*, 2016, **3**(8):887.

[11] POULTON C V, YAACOBI A, COLE D B, *et al*. Coherent solid-state LIDAR with silicon photonic optical phased arrays[J]. *Optics Letters*, 2017, **42**(20):4091-4094.

[12] SUN J, TIMURDOGAN E, YAACOBI A, *et al*. Large-scale nanophotonic phased array.[J]. *Nature*, 2013, **493**(7431):195-199.

[13] ROGIER H, ACOLEYEN K V, BAETS R. Two-dimensional optical phased array antenna on silicon-on-insulator[J]. *Optics Express*, 2010, **18**(13):13655.

[14] NIKKHAH H, ACOLEYEN K V, BAETS R. Beam steering for wireless optical links based on an optical phased array in silicon[J]. *Annals of Telecommunications-annales des Télécommunications*, 2013, **68**(1-2):57-62.

[15] WANG Ke, WANG Yang, GAO Shi-tao, *et al*. 2 × 2 silicon integrated optical phased array for beam steering applications[C]. IEEE International Topical Meeting on Microwave Photonics, 2015:1-4.

[16] SUN J, HOSSEINI E S, YAACOBI A, *et al*. Two-dimensional apodized silicon photonic phased arrays[J]. *Optics Letters*, 2014, **39**(2):367.

[17] ABIRI B, AFLATOUNI F, REKHI A, *et al*. Electronic two-dimensional beam steering for integrated optical phased arrays[C]. IEEE Optical Fiber Communications Conference and Exhibition, 2014:1-3.

[18] AFLATOUNI F, ABIRI B, REKHI A, *et al*. Nanophotonic projection system[J]. *Optics Express*, 2015, 23(16): 21012-21022.

[19] ABEDIASL H, HASHEMI H. Monolithic optical phased-array transceiver in a standard SOI CMOS process[J]. *Optics Express*, 2015, **23**(5):6509-6519.

[20] AFLATOUNI F, ABIRI B, REKHI A, *et al*. Nanophotonic coherent imager[J]. *Optics Express*, 2015, **23**(4):5117-5125.

[21] CHEN X, THOMSON D J, CRUDGINTON L, *et al*. Dual-etch apodised grating couplers for efficient fibre-chip coupling near 1 310 nm wavelength.[J]. *Optics Express*, 2017, **25**(15):17864-17871.

[22] NIU D, SUN S, XU Q, *et al*. Optimized design and fabrication of polymer/silica thermo-optic switch with low power consumption.[J]. *Applied Optics*, 2017, **56**(21):5799-5803.

[23] KIM J H, YOU J B, PARK J H, *et al*. Design of nano-photonic phased-array antennas for wide-angle beam-steering [C]. International Conference on Advanced Communication Technology. IEEE, 2016:422-425.

[24] HE L, LIU Y, GALLAND C, *et al*. A high-efficiency nonuniform grating coupler realized with 248-nm optical lithography[J]. *IEEE Photonics Technology Letters*, 2013, **25**(14):1358-1361.

[25] WALDHÄUSL R, SCHNABEL B, DANNBERG P, *et al*. Efficient coupling into polymer waveguides by gratings[J]. *Applied Optics*, 1997, **36**(36):9383-9390.

[26] SKOLNIK M I. Introduction to radar systems[M]. 2nd edition. McGraw-Hill, 1980.

引用格式:LI Zhong-yu, ZHANG Ling-xuan, ZENG Chao, *et al*. Ultra-wide Two-dimensional Beam Steering by Silicon Integrated Optical Phased Array[J]. *Acta Photonica Sinica*, 2018, **47**(9):0913003

李中宇,章羚璇,曾超,等.基于硅基光学相控阵的大范围二维光束扫描[J].光子学报,2018,**47**(9):0913003